Title:

Experimental investigation on cylindrically macro-encapsulated latent heat storage for space heating applications

Authors and Affiliations

Tianhao Xu[1*], Justin Ningwei Chiu[1], Björn Palm[1], Samer Sawalha[1]

1 Department of Energy Technology, KTH Royal Institute of Technology, 100 44, Stockholm, Sweden

*Corresponding authors. Tel.:+46 (0) 72 032 5022; E-mail addresses: txu@kth.se

Abstract

The integration of latent heat thermal energy storage (LHTES) units with heating systems in buildings is regarded as a promising technology for heating load management; however, so far a limited number of experimental studies have been reported that focus on space heating applications on a representative scale. In this study, we develop and test a 0.38 m^3 LHTES unit containing cylindrically macro-encapsulated phase change materials (PCMs) with a melting temperature range of 44 to 53 °C and with gross mass of 154 kg. The unit has been tested with two tank orientations, horizontal and vertical. In the horizontal orientation tests, parametric studies show that increasing the difference between heat transfer fluid (HTF) supply temperatures and phase-change temperatures of PCMs, as well as increasing HTF flowrates, can both reduce the complete melting/solidification and complete charging/discharging time. Non-linear charging/discharging rates in PCMs are observed. The vertical orientation enables the forming of either a stratified or mixed flow regime in the tank. For charging, the stratified flow provides higher charging rates in PCMs compared to the mixed flow. When discharging the unit with a stratified HTF flow at 35 °C, lower HTF flowrates prolong the discharging time during which the released heat sustains an outlet temperature above 45 °C. Finally, comparisons between horizontal and vertical orientation tests reveal that although the vertical orientation can shorten the charging/discharging time by up to 20% for the entire unit to reach an energy density of 30 kWh/m^3, it leads to decrease in PCM thermal capacity by at most 8.2%. The speculated cause of this loss is phase segregation suggested by observed fluid motions in PCM cylinders. This study comprehensively characterizes an LHTES unit providing insights to optimizing its operating strategies considering its coupling with space heating systems.

Key words

Phase change material; Thermal energy storage; Space heating applications; Experimental study; Cylindrical encapsulation

Nomenclature

$\dot{V}$	volumetric flowrate [m^3/h]
c_p	specific heat [kJ/(kg·K)]
h	global heat transfer coefficient [kW/(m^2·K)]
k	thermal conductivity [W/(m·K)]
P	charging/discharging rate [kW]
Q	thermal capacity [kWh]
q	volume-specific thermal capacity, $q=Q/V$ [kWh/m^3]
Re	Reynolds number
S	surface area of the storage tank [m^2]
T	temperature [°C]
t	time [hours]
V	volume [m^3]

Greek symbols

ρ	density [kg/m^3]
Δ	relative difference [%]

Superscripts

30 kWh/m^3	the status when volume-specific thermal capacity reaches 30 kWh/m^3
75%/90%	the status when PCM thermal capacity reaches 75%/90% of its theoretical maximum value

Subscripts

av	average value
c	charging
com	completely charged/discharged status
d	discharging
in	inlet condition
ini	initial status
l	liquid phase
loss	heat loss
out	outlet condition
pk	peak value
s	solid phase
sen	sensible heat

spl	supply condition
sur	surrounding air
TES	for the entire thermal energy storage unit
theo	theoretical values

Abbreviations

A/C	air-conditioning
DOT	design outdoor temperature
DSM	demand-side management
HTF	heat transfer fluid
LHTES	latent heat thermal energy storage
PCM	phase change material

39

1. Introduction

Building sectors constitute 40% of the total energy demand in the European Union [1], while in the EU-15 electricity use in the residential and tertiary sectors accounts for about 50% [2]. It is deemed beneficial to apply demand-side management (DSM) strategies in buildings to enable the utilization of more energy-efficient devices and more renewable energy as the source [3]. Thermal energy storage (TES) is regarded as one of the key technologies of DSM to shape loads and to increase the utilization of renewable energy for both heating and cooling in buildings [4]. The major part of energy use (more than 50%) in buildings goes to space heating in the European context; this portion was reported to be more than 60% in Northern European countries such as Denmark, Norway and Iceland [5]. Peak shaving on the heating load in buildings through demand-side TES devices can potentially reduce operating costs for end users and simultaneously promote energy generating efficiency for energy suppliers [6].

Among different technologies of TES, the use of phase change materials (PCMs) in the application of short-term storage is attractive due to their high energy storage density and small temperature swing comparing to sensible thermal energy storage [7]. As a DSM tool that can be actively coupled to building energy systems, a latent heat thermal energy storage (LHTES) unit is ideally featured with high energy density, simplicity, compatibility, and reliability [8]. For applications of space-heating load management, one of the most common implementation strategies is to actively integrate such units with hydronic space heating systems, in which the heat is provided by district heating, heat pumps, electric boilers, or fossil-fuel boilers and carried by the water to be distributed to heating terminals through pumping [4]. Before an LHTES unit is implemented, two aspects that need to be considered are: proper selection of (1) the PCM and (2) the storage configuration of the unit.

For the selected PCM, its melting and solidification point should be well considered to suit the operational temperature of hydronic space heating systems. By reviewing the case in Sweden, it is found that radiator systems are most common and their supply temperature is normally determined by the heating curve according to the ambient air temperature [9]. A recent study summarized the typical operational temperature for hydronic radiator systems in Northern European countries; the water supply temperatures were reported within the range of 45 to 55 °C during major periods of a year [10]. In Sweden, design supply temperature has been restricted below 55 °C for most cases by building regulations since 1982 [11]. According to Swedish heat pump manufacturers, the supply and return temperatures of 55 °C and 45 °C, respectively, at the design outdoor temperature (DOT) of -20 °C are chosen for modern hydronic radiator systems [12]. Therefore, this typical temperature range for operating radiator systems (45 to 55 °C) narrows the selection of compatible PCMs to a few salt hydrates and paraffins with suitable phase-change temperatures. Limited amounts of commercial salt hydrates such as Climsel C48, STL47, and E48, as well as commercial paraffins such as RT50 and RT52, are available on the market [13].

Moreover, suitable PCMs for space heating applications should also possess desirable thermo-physical and chemical properties. Two major categories of PCMs, salt hydrates and paraffins, have been compared in terms of thermo-physical and chemical properties in several review articles [13, 14]. Compared to paraffins, salt hydrates have higher thermal conductivity and latent heat of fusion, which are the desirable thermo-physical properties to achieve high charging/discharging thermal power rate and storage capacity for an LHTES unit. Nevertheless, many of the salt hydrates have some intrinsic drawbacks during phase-change, such as supercooling and phase segregation, which impede the retrieval of thermal energy when the PCMs solidify. Segregation can be prevented by adding gelling agents or thickeners [15]; this measure has been implemented in many commercial PCM products.

On the other hand, PCMs should be contained in a sealed and efficient way to exchange heat with heat transfer fluids (HTFs). Two main PCM containments are typically used in active storage systems: (1) bulk storage of PCMs in a specific heat exchanger or (2) placement of encapsulated PCMs in a storage unit such as a packed bed [16]. The former is commonly integrated with a shell-and-tube heat exchanger, where PCMs are kept in the shell and HTFs flow in the pipe to release and absorb heat [17, 18]. The principle of the latter method involves the flow of HTFs over the encapsulation surface to exchange heat with the macro-encapsulated PCMs, which are tightly packed in the storage container. The second type of LHTES configurations has been widely applied in the industry for the built environment and a number of manufacturers are producing macro-encapsulated PCMs dedicated for such storage units [19].

For PCM bulk storage, a considerable number of experimental studies on the thermal performance of LHTES have been investigated; the majority of the tested units adopted a shell-and-tube design and employed organic PCMs as the storage media. Amongst these studies, some are dedicated for the application of active integration with hydronic heating systems. For example, Agyenim and Hewitt [20] developed a 1.2 m long copper cylinder with longitudinal fins and tested RT58, a commercial paraffin, in a test facility incorporating a hot water radiator. A 140 L compact PCM storage tank with two submerged coils was developed by Martin and Setterwall [21] for solar heating applications; a commercial salt-based PCM with a melting point of 58 °C was evaluated by its heat transfer performance in the storage tank. Hosseini et al [22] examined the thermal performance of RT50, a commercial paraffin that completely melts above 51 °C, in a 1.0 m long finned cylinder with different fin heights and HTF inlet temperatures. Rathod and Banerjee [23] introduced a 1.0 m high PCM-tank for storing heat produced by solar water heaters; the employed PCM is stearic acid of which the melting temperature is 57.5 °C. Specially, a 1.5 m high cylindrical storage tank containing

116 kg sodium acetate trihydrate composites was investigated by Dannemand et al. [18] to utilize the stable supercooling of PCMs for seasonal heat storage.

Unlike the abovementioned experimental studies tested on large scales, some recent work [17, 24-27], despite focusing on the active heating applications, developed PCM heat exchangers on a considerably smaller scale (PCM mass in LHTES is less than 10 kg) mainly for the purpose of validating the phase-change models.

For the storage configuration with macro-encapsulated PCMs, some researchers tested PCM cylinders with diameters between 50 mm and 70 mm and lengths from 300 mm to 750 mm [28-31]. Other researchers focused on spherical containers with diameters ranging from 28 mm to 77 mm [32-38]. Additionally, a rectangular storage tank containing macro-encapsulated PCMs flat slabs with dimension of 500 mm × 250 mm × 32 mm was investigated [39]. Three types of applications were primarily considered for these experimental studies: (1) high-temperature applications using molten salt as PCMs for solar heat storage on the power generation side [30, 33]; (2) air-conditioning (A/C) applications using paraffins or salt hydrates for indoor comfort cooling [32, 36, 37, 39]; and (3) water heating applications using paraffins or salt hydrates mainly for storing solar heat [28, 29, 31, 38], which basically suit the operating temperature of radiator heating systems. These studies mainly presented experimental results of the temperature evolution of a PCM and an HTF during the charging/discharging processes.

On the other hand, one experimental investigation stands out [32] as it detailed the effects from the HTF supply conditions on charging/discharging rates and total stored/released heat capacity over the complete charging/discharging timespan in a lab-size storage tank (1 m^3), which was scaled down from an industrial tank (up to 500 m^3). These parameters—rate, capacity, and time—which indicate the thermal performance of an LHTES, should be well

understood under different working conditions, such as HTF supply temperatures and flowrates. However, a limited number of previous experimental studies have delved into comprehensively evaluating these parameters of a macro-encapsulated LHTES unit, especially for heating applications.

To extend such experimental investigations for heating applications, the present study develops and experimentally characterizes a large-scale LHTES unit containing cylindrically macro-encapsulated PCMs. Key thermal performance indicators are characterized under different HTF supply conditions for two tank orientations, horizontal and vertical. Climsel C48 was employed as the PCM as the operating performance analysis of this commercial product for large scale active heating applications has not been widely reported in scientific articles. This work also provides insights on desirable operating strategies when integrating LHTES units with hydronic space heating systems.

2. Methodology

2.1. Test facility for encapsulated PCMs

For the containment of encapsulated PCMs, a cylindrical LHTES tank made of stainless steel type 316 with an outer diameter of 606 mm and a length of 1350 mm was designed and produced, as displayed in Fig. 1. The tank was designed with flow distributors at both ends and can be mounted either horizontally or vertically to study the effects of orientation on the unit's performance. The HTF flows in the channels formed by the arbitrary array of encapsulated PCM cylinders.

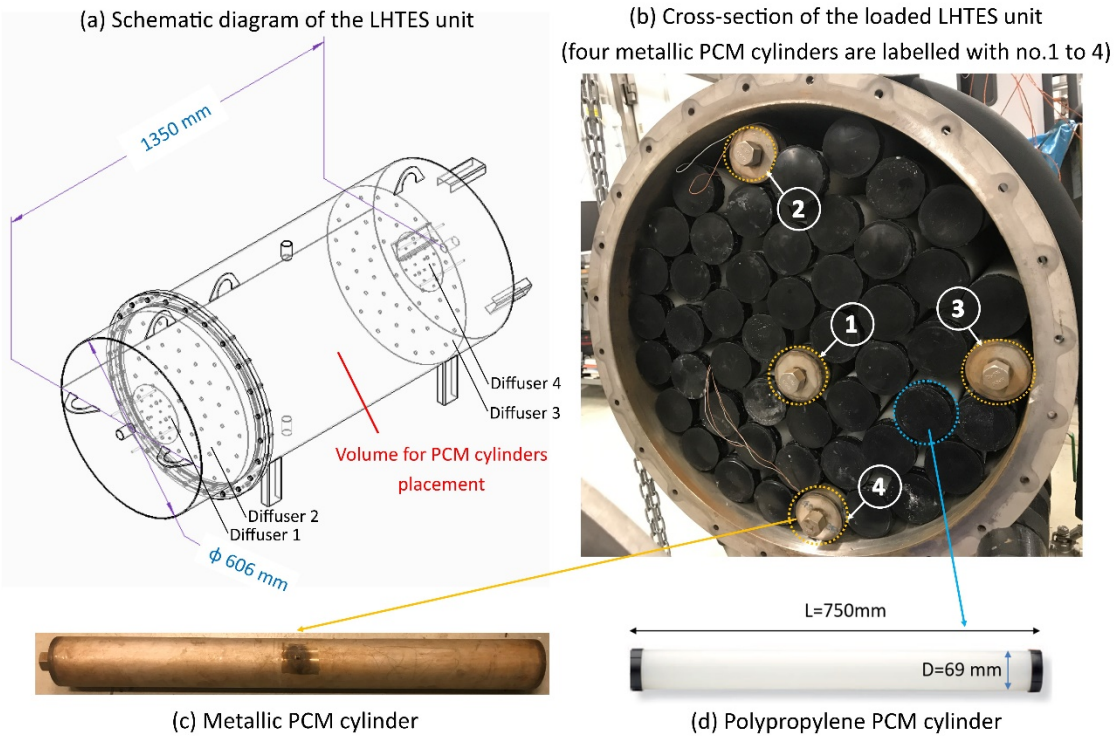

Fig. 1. Illustration of LHTES unit and encapsulated PCM cylinders.

The hydraulic test facility regulating the HTF's conditions is coupled to the LHTES unit. A schematic diagram of the complete test facility is provided in Fig. 2. A PID-controlled electric heater, denoted by H in Fig. 2, provides controllable amounts of heat to the HTF, and a fin-and-coil heat exchanger (Q) removes redundant heat from the HTF in the hydraulic system. A four-way directional diverting valve (F) enables the change of HTF flow direction and a by-pass loop configured with a pressure-drop regulating valve (B) allows a desired HTF supply temperature to be set before the HTF enters the LHTES tank. The heat pump was designed to cool down the HTF for testing PCMs for A/C applications; thus, it was not activated in this study.

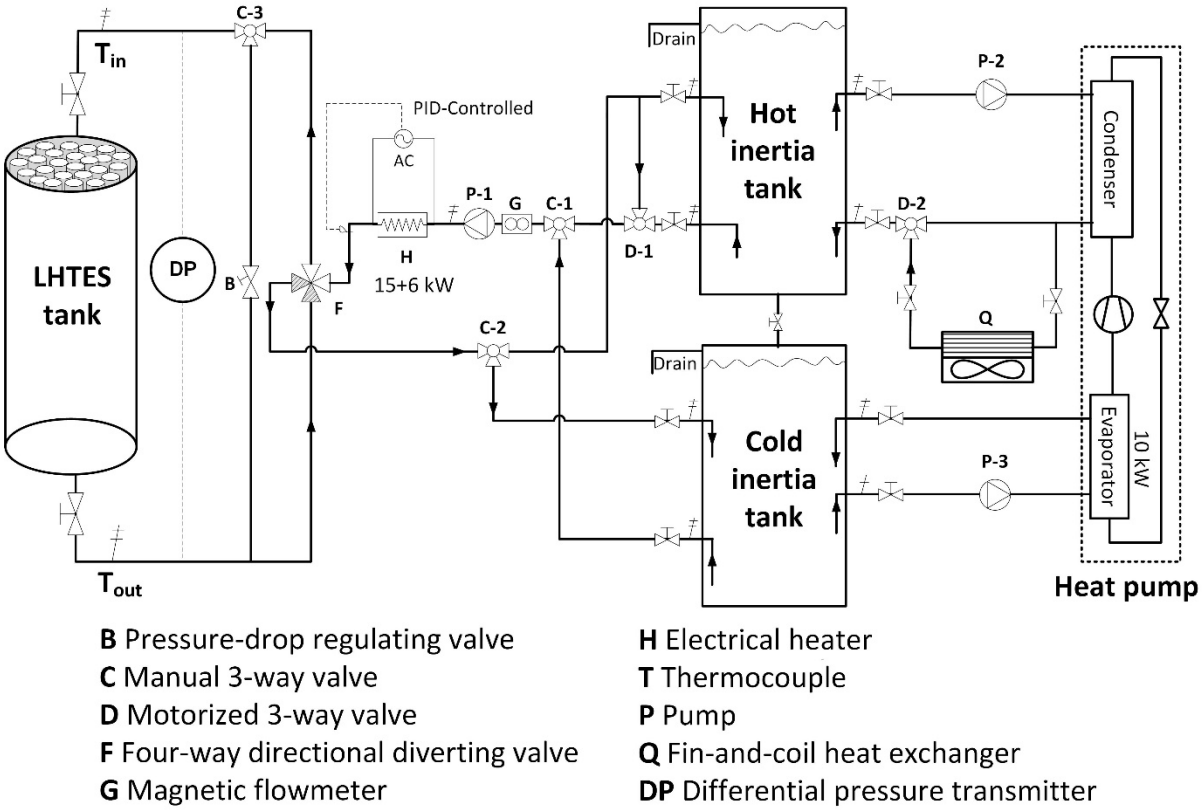

Fig. 2. Schematic diagram of the test facility.

2.2. Macro-encapsulated PCM products

Macro-encapsulation differs in materials, shapes, and sizes depending on the manufacturer. Although spherical containers for PCMs are proved to have the highest heat transfer rate compared to other shapes [40], using plastic cylinders for macro-encapsulation is considered one of the most cost-effective solutions. In the present study, a cylindrical macro-encapsulated PCM product with a length of 750 mm and an outer diameter of 69 mm was tested in the aforementioned experimental apparatus (see Fig. 1d). The encapsulation is made of polypropylene with a thickness of 1 mm. The volume of each encapsulated cylinder is 2.8 $\times 10^{-3}$ m^3. As shown in Fig. 1(b), the tank is loaded with 50 encapsulated PCM cylinders. PCM cylinders occupy about 58% of the volume for PCM cylinder placement, and 37% of the

total volume of the storage tank as the inlet and outlet sections designed with diffusers are only filled with HTFs (see Fig. 1a). The total mass of PCMs is 154 kg. The employed PCM is Climsel C48, which is a commercial product with well-defined thermo-physical properties (Table 1). This PCM stores latent heat in the temperature span between 44 and 53 °C during the melting process and releases latent heat between 48 and 41 °C when solidified, according to the specific heat curve provided by the manufacturer [41].

Table 1 Thermo-physical properties of Climsel C48 [41].

Parameters	Value
Phase-change temperature (melting)	44 to 53 °C
Phase-change temperature (solidification)	48 to 41 °C
Latent heat of fusion ($Q_{PCM,theo}$) [40 to 55 °C]	180 kJ/kg
Thermal conductivity: solid (k_s)	0.76 W/(m·K)
Thermal conductivity: liquid (k_l)	0.53 W/(m·K)

2.3. Measurement

Three parameters are measured to characterize the HTF's conditions: temperature, volumetric flowrate, and pressure drop. The temperature sensors are T-type thermocouples. The accuracy of the thermocouples at the inlet and outlet of the LHTES unit, denoted by T_{in} and T_{out}, respectively, in Fig. 2, was tested by comparison to a calibrated precision digital thermometer between 30 and 70 °C with a temperature interval of 2 °C; the mean deviation is below 0.05 °C. Volumetric flowrate is measured with a magnetic flowmeter (Yokogawa RXF); the relative measurement error of the reading is $\pm$ 0.5% [42]. The pressure drop across the tank is measured by a differential pressure transmitter (Yokogawa EJA 110 A) [43].

For measuring interior PCM temperatures, four stainless steel type 316 cylinders were fabricated with the same dimensions as the plastic cylinders. These cylinders contained thermowells for thermocouple installation. The arrangement of the four cylinders in the LHTES unit is shown in Fig. 1(b): one cylinder with four thermowells (cylinder 1) is at the center of the tank and the other three cylinders, with only one thermowell each (cylinders 2, 3 and 4), are at the circular perimeter. The positions of PCM temperature measurements (T_{PCM1} to T_{PCM7}) are illustrated in Fig. 3. Stainless steel cylinders were used for the ease of thermocouples insertion and monitoring. A simplified model was created to investigate the influence of the stainless steel on the heat transfer to PCMs as compared to polypropylene cylinder tubes. Results show that the required phase change time differs by about 3% between the two cases, furthermore the preciseness in positioning and tight-sealing justifies the use of stainless steel cylinders for PCM temperature measurements.

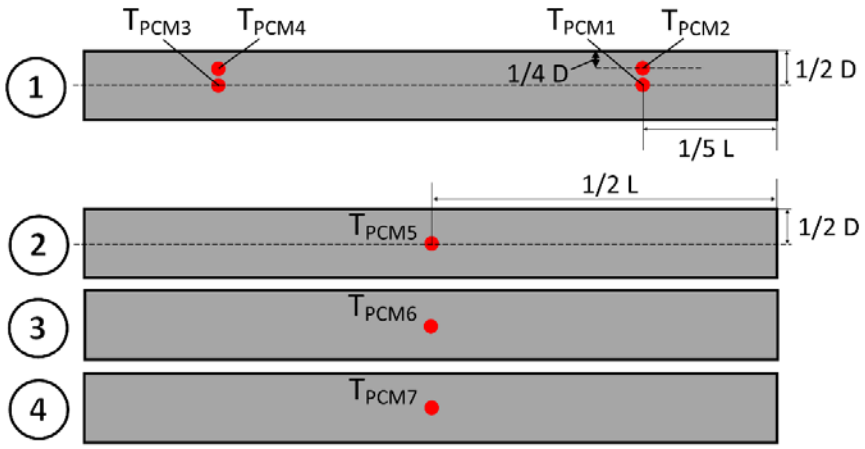

Fig. 3. PCM temperature measurement positions in metallic PCM cylinders.

2.4. Experimental procedures

Charging/discharging tests are based on constant HTF supply conditions. Before each test started, the initial temperature of both the PCM and the accumulated HTF volume in the

LHTES unit were maintained at a fixed temperature, $T_{TES,ini}$. During a test, the HTF was pumped to the LHTES unit with a fixed temperature ($T_{HTF,spl}$) and a fixed volumetric flowrate ($\dot{V}_{HTF}$). The test was considered complete when the temperature difference between HTF inlet (T_{in}) and HTF outlet (T_{out}) leveled off, which depends on the HTF flowrate, e.g., 0.15 °C for $\dot{V}_{HTF}$ = 1.5 m^3/h.

2.5. Data reduction and uncertainty analysis

Charging/discharging rates are introduced to describe the transient thermal performance of the LHTES unit. The charging/discharging rate (P_{TES}) is calculated according to the measured temperature difference ($T_{in} - T_{out}$) of the HTF over the LHTES unit, which can be expressed as the first term in Eq. (1). However, this temperature difference includes the effect of heat loss from the unit to the surroundings. The heat loss effect, termed as P_{loss}, is thus subtracted in Eq. (1) from the heat balance to calculate the actual charging/discharging rates.

$$P_{TES} = \left| \rho_{HTF} \cdot \dot{V}_{HTF} \cdot c_{p_{HTF}} \cdot (T_{in} - T_{out}) - P_{loss} \right| \quad (1)$$

The heat loss is experimentally determined by homogenously maintaining the tank at fixed temperatures for at least 10 hours and calculating the energy balance. The bulk temperature is represented by the mean HTF temperature ($T_{HTF,av}$) throughout the unit. Using an integral term, $h_{loss}S$, which is the product of the global heat transfer coefficient of heat loss and tank surface area, to linearly correlate the heat loss with the temperature difference between the unit and the surroundings, the unit's heat loss was characterized from 25 °C to 60 °C with a temperature interval of 5 °C in Eq. (2). The experimentally obtained $h_{loss}S$ equals 7.4 W/K for this unit.

$$P_{loss} = h_{loss}S \cdot (T_{HTF,av} - T_{sur}) \quad (2)$$

The thermal capacity of the LHTES unit is composed of two parts: (1) the heat stored in or recovered from the encapsulated PCMs (Q_{PCM}) and (2) the HTF volume accumulated in the tank (Q_{HTF}). The thermal capacity is the accumulation of charging/discharging rates in a defined period ($Q_{TES} = \int_{t_1}^{t_2} P_{TES}\, dt$). Hence, the thermal capacity of PCMs can be calculated according to Eq. (3). The heat content of the polypropylene encapsulation is neglected due to its small volume.

$$Q_{PCM} = Q_{TES} - Q_{HTF} \tag{3}$$

In this equation, the sensible heat stored/released by the gradual replacement of HTF volume with that at higher/lower temperature during charging/discharging in the defined period can be calculated with the mean bulk temperature difference, see Eq. (4).

$$Q_{HTF} = \rho_{HTF} \cdot \dot{V}_{HTF} \cdot c_{p_{HTF}} \cdot \left| T_{HTF,av,t_2} - T_{HTF,av,t_1} \right| \tag{4}$$

Uncertainties in the calculated parameters, such as the charging/discharging rates and thermal capacity, are due to measurement uncertainty. Depending on the test condition ($T_{HTF,spl}$, $T_{TES,ini}$, and $\dot{V}_{HTF}$), expanded uncertainties with a confidence level of 95% are obtained for peak/average P_{TES} and accumulated Q_{TES} according to the NIST guidelines for uncertainty evaluation [44]; they are listed in Table 2.

Table 2 Uncertainty analysis for charging/discharging rates and thermal capacity.

Test conditions			**Expanded uncertainty with 95% of confidence level**		
$T_{HTF,spl}$ [°C]	$T_{TES,ini}$ [°C]	$\dot{V}_{HTF}$ [m^3/h]	$P_{TES,pk}$ [kW]	$P_{TES,av}$ [kW]	$Q_{TES,com}$ [kWh]

	55	35	0.5	±0.12	±0.02	±0.19
	55	35	1.5	±0.33	±0.05	±0.44
Charging	55	35	4.0	±0.92	±0.11	±0.79
	58	35	1.5	±0.44	±0.05	±0.35
	60	35	1.5	±0.42	±0.05	±0.34
	35	55	0.5	±0.11	±0.02	±0.18
	35	55	1.5	±0.34	±0.05	±0.37
Discharging	35	55	4.0	±1.04	±0.11	±0.82
	40	55	1.5	±0.25	±0.04	±0.44
	30	55	1.5	±0.43	±0.05	±0.26

3. Horizontal orientation tests

The horizontal orientation of the LHTES unit was investigated since such a configuration has been widely applied in industrial applications for containing macro-encapsulated PCMs due to the convenience of installation [45, 46]. The charging/discharging thermal performance under various HTF supply conditions is presented in the following section as a parametric study.

3.1. Charging mode

Effects of the HTF supply temperature ($T_{HTF,spl}$) at 55, 58 and 60 °C (C48 has been reported to degrade above 60 °C), and of the volumetric flowrate ($\dot{V}_{HTF}$) at 0.5, 1.5 and 4.0 m^3/h, are shown in Fig. 4(a) and (b), respectively. Two parameters are presented with their evolution during charging: (1) the charged thermal capacity of the entire LHTES unit, Q_{TES}, and (2)

263 $T_{PCM,av}$, which is the mean value of five measured PCM temperatures (T_{PCM1}, T_{PCM3}, T_{PCM5},
264 T_{PCM6}, and T_{PCM7}) at the center of cylindrical cross-section. For gelled PCMs, conduction
265 dominates the heat transfer mechanism; thus, the internal convective heat transfer is negligible,
266 primarily due to its high viscosity [47, 48]. The cross-sectional center of a long cylinder is
267 regarded to represent the lowest-temperature position during charging. Therefore, when
268 $T_{PCM,av}$ reaches 53 °C, which is the liquidus temperature of C48, the PCM is considered to be
269 completely melted.

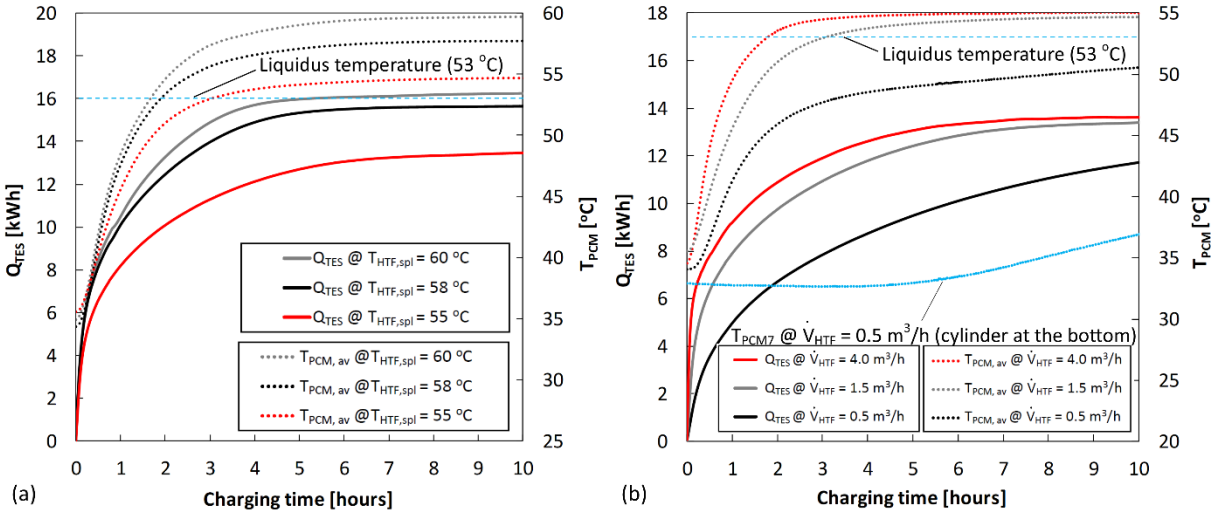

270

271 **Fig. 4.** The evolution of PCM temperature and charged thermal capacity with different HTF supply conditions
272 for charging: (a) $T_{HTF,spl}$ of 55, 58 and, 60 °C at 1.5 m^3/h ($T_{TES,ini}$ at 35 °C); (b) $\dot{V}_{HTF}$ of 0.5, 1.5 and, 4.0 m^3/h with
273 $T_{HTF,spl}$ of 55 °C ($T_{TES,ini}$ at 35 °C).

274

275 Experimental data in Fig. 4 illustrate two main findings. First, shorter complete melting and
276 charging time can be achieved by increasing $T_{HTF,spl}$ from 55 to 58 and 60 °C and $\dot{V}_{HTF}$ from
277 0.5 to 1.5 and 4.0 m^3/h. The second experimental finding, depicted in Fig. 4(b), is that with
278 $\dot{V}_{HTF}$ equal to 0.5 m^3/h, the core PCM of the cylinder placed at the bottom of the LHTES unit
279 (see T_{PCM7}), underwent insufficient heating from the inlet HTF flow, showing a much lower
280 measured temperature relative to the other cylinders within a 10-hour charging time. The

warm inlet HTF flow with a small flowrate, though designed to be uniformly distributed by diffusers, tended to ascend to upper regions causing insufficient flow to the bottom, owing to the relatively stronger free convection compared to forced convection. Such distribution problems led to a reduced Q_{TES}.

A summary of the experimental results for the five test conditions presented in Fig. 4, focused on Q_{TES}, Q_{PCM}, q_{TES} (defined as volume-specific thermal capacity of the entire unit) and charging time, is shown in Table 3. For easy comparison, the test condition of $T_{HTF,spl}$ = 55 °C, $T_{TES,ini}$ = 35 °C and $\dot{V}_{HTF}$ = 1.5 m^3/h is defined as the reference charging condition. First, when $T_{HTF,spl}$ increased from 55 to 60 °C, both Q_{TES} and Q_{PCM} increased obviously due to the rise in stored sensible heat. Also, the time for complete melting, for complete charging, and for q_{TES} reaching 30 kWh/m^3 (q_{TES} = 30 kWh/m^3 is defined as a criterion for evaluating the storage density of the entire LHTES), was reduced by 43%, 15%, and 61%, respectively, by elevating $T_{HTF,spl}$ from 55 to 60 °C. This is because an increased temperature difference between HTF and PCMs improved the driving force for heat transfer. Second, compared to the reference, increasing $\dot{V}_{HTF}$ to 4.0 m^3/h achieved reductions in complete melting (40%) and charging time (15%); time for q_{TES} to reach 30 kWh/m^3 decreased as well from 3.6 to 2.5 hours. However, decreasing $\dot{V}_{HTF}$ to 0.5 m^3/h led to incomplete charging of the LHTES unit even after 16 hours of charging; Q_{PCM} approached only 12.8 kWh, 9% less compared to that of the reference. Based on the results in Table 3, it can be concluded that the charging thermal performance can be improved by increasing HTF supplying temperatures and flowrates.

Table 3 Charging thermal performance with different test conditions for the horizontal LHTES orientation.

Parameters	Test conditions

	1[a]	2	3	4	5
$T_{HTF,spl}$ [°C]	55	58	60	55	55
$T_{TES,ini}$ [°C]	35	35	35	35	35
$\dot{V}_{HTF}$ [m^3/h]	1.5	1.5	1.5	0.5	4.0
$t_{c,com}$ [hours]	8.2	7.2	7.0	-	7.0
$Q_{TES,com}$ [kWh]	13.3	15.6	16.1	12.8[c]	13.7
$\Delta Q_{TES,com}$ [b] [%]	-	+13.5%	+17.4%	-3.8%[c]	+3.0 %
$q_{TES,com}$ [kWh/m^3]	34.8	40.7	42.1	33.5[c]	35.8
$Q_{PCM,com}$ [kWh]	8.5	9.6	9.8	7.7[c]	8.7
$t_{m,com}$ [hours]	3.0	1.9	1.7	-	1.8
$t(q_{TES}^{30\ kWh/m^3})$ [hours]	3.6	1.7	1.4	9.2	2.5

[a] Reference charging condition.

[b] Compared to the reference charging condition.

[c] No complete melting/charged condition reached, values after 16-hour charging presented for $\dot{V}_{HTF}$ = 0.5 m^3/h.

3.2.Discharging mode

Similar to the charging mode, discharging tests were conducted with three levels of $T_{HTF,spl}$ (30, 35, and 40 °C, respectively) and three different $\dot{V}_{HTF}$ values (0.5, 1.5, and 4.0 m^3/h); $T_{TES,ini}$ was kept at 55 °C. In Fig. 5, development of Q_{TES} and $T_{PCM,av}$ during discharging is presented. Two key findings can be extracted from the comparisons: (1) complete solidification and discharging time is shortened by decreasing $T_{HTF,spl}$ or increasing $\dot{V}_{HTF}$; (2) with $\dot{V}_{HTF}$ = 0.5 m^3/h, the top cylinder underwent insufficient cooling due to the uneven HTF

distribution. Details of the five discharging test conditions are provided in Table 4. Comparisons of time for complete solidification, complete discharging, and q_{TES} reaching 30.0 kWh/m^3 indicate the same experimental findings as charging: increasing the temperature difference between HTF and PCM and increasing $\dot{V}_{HTF}$ improves the heat transfer rate and accelerates the discharging process.

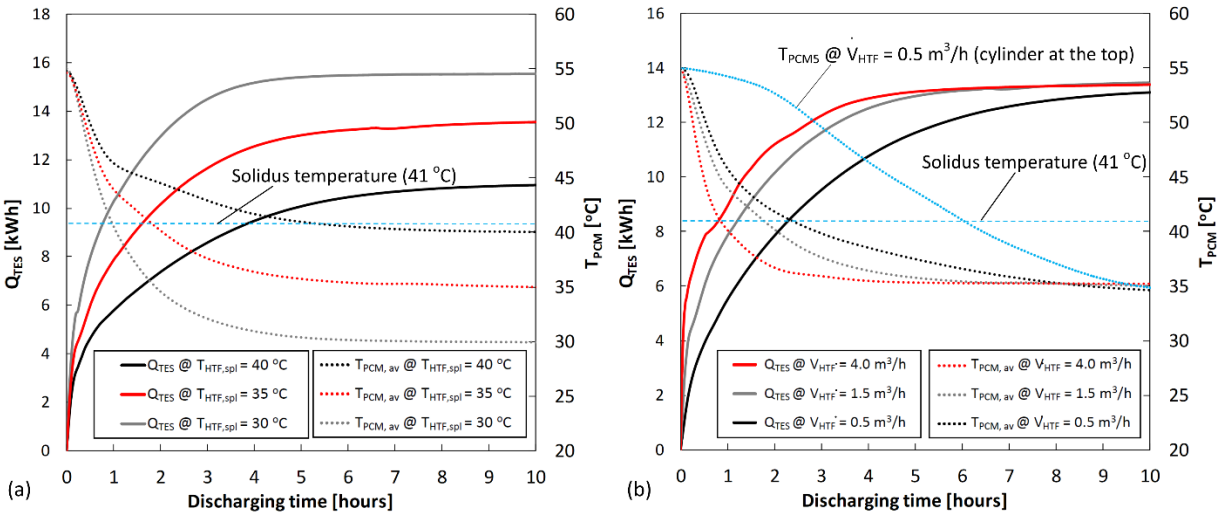

Fig. 5. The evolution of PCM temperature and discharged thermal capacity with different HTF supply conditions for discharging: (a) $T_{HTF,spl}$ of 30, 35, and 40 °C at 1.5 m^3/h ($T_{TES,ini}$ at 55 °C); (b) $\dot{V}_{HTF}$ of 0.5, 1.5, and 4.0 m^3/h with $T_{HTF,spl}$ of 35 °C ($T_{TES,ini}$ at 55 °C).

Table 4 Discharging thermal performance with different test conditions for the horizontal LHTES orientation.

Parameters	Test conditions				
	1[a]	2	3	4	5
$T_{HTF,spl}$ [°C]	35	40	30	35	35
$T_{TES,ini}$ [°C]	55	55	55	55	55

$\dot{V}_{HTF}$ [m^3/h]	1.5	1.5	1.5	0.5	4.0
$t_{d,com}$ [hours]	8.3	10.9	4.8	10.0	7.2
$Q_{TES,com}$ [kWh]	13.5	11.1	15.5	13.2	13.4
$\Delta Q_{TES,com}$ [b] [%]	-	-17.0%	+16.8%	-2.2%	-0.1%
$q_{TES,com}$ [kWh/m^3]	35.2	29.2	41.0	33.5	35.2
$Q_{PCM,com}$ [kWh]	8.5	7.3	9.4	8.0	8.5
$t_{s,com}$ [hours]	1.8	5.0	1.0	2.4	0.9
$t(q_{TES}^{30\ kWh/m^3})$ [hours]	2.9	-	1.4	4.8	2.3

[a] Reference discharging condition.

[b] Compared to the reference discharging condition.

3.3.Discussions of LHTES horizontal orientation tests

PCM thermal capacity (Q_{PCM}) comprises more than 60% of the total thermal capacity of the entire unit (Q_{TES}). To generally demonstrate charging/discharging rates in PCMs for horizontal orientation tests, Fig. 6(a) and (b) illustrate how Q_{PCM} developed during charging and discharging, respectively, for all test conditions. Each curve represents a single test condition with fixed $T_{HTF,spl}$, $T_{TES,ini}$, and $\dot{V}_{HTF}$. The three points on each curve represent times when Q_{PCM} reached 75, 90, and 99%, respectively, of the theoretically maximum charging/discharging thermal capacity, $Q_{PCM,theo}$. The maximum capacity was calculated according to the manufacturer's method [55], considering the temperature range (from $T_{TES,ini}$ to $T_{HTF,spl}$) for each test condition. Also, the Reynolds number for each $\dot{V}_{HTF}$ is shown in the legend; the HTF flow is laminar for all test conditions. The most time-efficient charging condition is for $T_{HTF,spl}$ = 60 °C and $\dot{V}_{HTF}$ = 4 m^3/h (Re=575), as shown in Fig. 6(a). For this

condition, charging time, compared to the reference charging condition, is reduced by 53% for the point when Q_{PCM} reached 99% of $Q_{PCM,theo}$. Similarly, it can be observed in Fig. 6(b) that the shortest discharging time compared to the reference occurs for the condition of $T_{HTF,spl}$ = 30 °C and $\dot{V}_{HTF}$ = 4 m^3/h; the discharging time decreased by 32%. In addition, the maximum pressure drop across the LHTES unit was measured to be 831.6 Pa for charging and 925.7 Pa for discharging with $\dot{V}_{HTF}$ of 4 m^3/h.

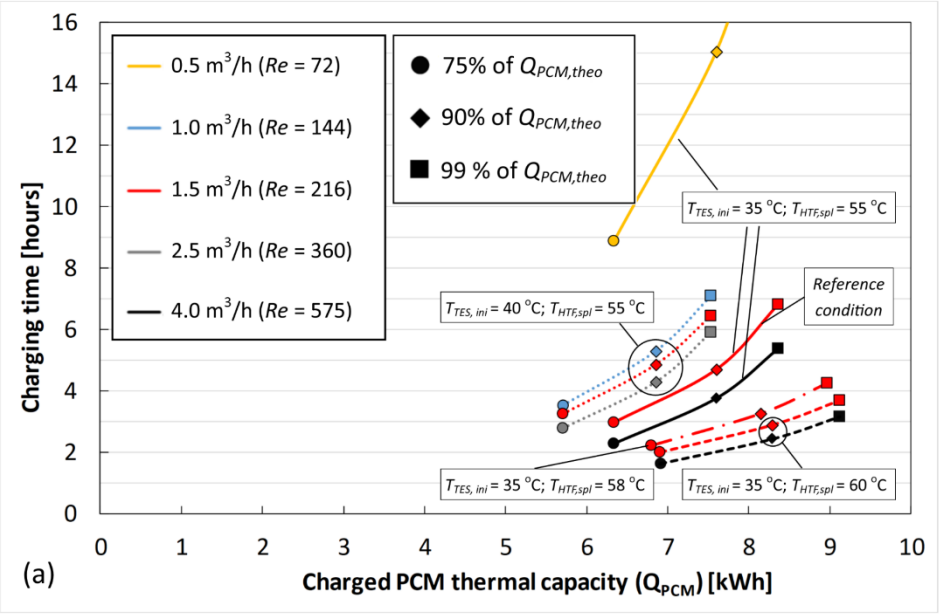

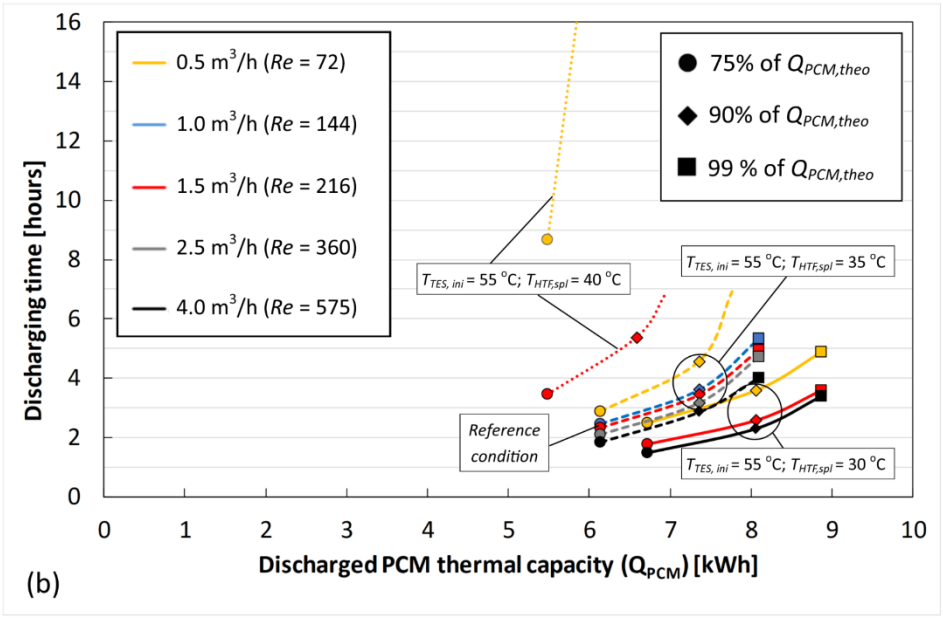

Fig. 6. Generalized performance map of charging/discharging rates in PCMs with horizontal LHTES orientation: (a) charging; (b) discharging.

Data for partial-load status is also shown in Fig. 6. Charging time is found to increase non-linearly from the point of 75 – 90% $Q_{PCM,theo}$ to the point of 99% $Q_{PCM,theo}$. For instance,

charging time can be shortened from 6.8 to 3.0/4.7 hours, 56%/31% less, if only 75%/90% of $Q_{PCM,theo}$ was desired instead of 99% $Q_{PCM,theo}$, for the reference charging condition. For the reference discharging condition, the time was reduced from 4.9 to 2.3/3.5 hours (53%/30% reduction) for 75%/90% $Q_{PCM,theo}$. Correspondingly, Q_{TES} decreased by 17%/7% for 75%/90%-$Q_{PCM,theo}$ compared to 99% $Q_{PCM,theo}$. This observed non-linearity of charging/discharging rates in PCMs implies that partial loads can significantly shorten cycle times. Operating an LTHES unit using the tested encapsulated PCMs in a practical heating system can become time-efficient when leaving small parts of PCM thermal capacity uncharged/undischarged.

Some curves in Fig. 6(a) and (b) contain no square symbols, indicating a test condition at which the HTF was unable to store/recover up to 99% of $Q_{PCM,theo}$, regardless of charging/discharging time. This outcome can be either attributed to the uneven distribution of HTF flow, as discussed in Sections 3.1 and 3.2 where $\dot{V}_{HTF}$ was down to 0.5 m^3/h, or due to high $T_{HTF,spl}$ (40 °C), when the theoretical latent heat of fusion during discharging cannot be completely recovered.

4. Vertical orientation tests

The LHTES unit in the horizontal orientation with an HTF volumetric flowrate of 0.5 m^3/h or less produced an uneven distribution of HTF flow. To mitigate this undesirable condition, the LHTES unit was placed in vertical orientation aligning the gravitational force with the longitudinal direction of the tank. In the vertical orientation, no PCM cylinders were observed to suffer from inadequate heating/cooling due to non-uniform HTF flow. The charging mode was tested with two different flow directions, upward and downward, respectively, to investigate how flow direction affects thermal performance. Discharging tests were conducted with $\dot{V}_{HTF}$ as low as to 0.15 m^3/h in a stratified flow regime (HTF in upward direction). For

370 the tests presented in Sections 4.1 and 4.2, $T_{HTF,spl}$ and $T_{TES,ini}$ were fixed at 55 and 35 °C,
371 respectively, for each charging test, and 35 and 55 °C, respectively, for the discharging tests.

4.1.Charging mode

By triggering different flow regimes, different HTF flow directions can influence the charging thermal performance. Data in Fig. 7 indicate how T_{HTF2} and T_{HTF3}, HTF temperatures at two longitudinal positions along the PCM cylinder 1, developed during charging under four test conditions: with two different flow directions, upward and downward and with two different HTF flowrates, $\dot{V}_{HTF}$ = 0.5 m^3/h and 1.5 m^3/h. For both flowrates, a mixed HTF flow formed with upward flow while the downward flow produced a stratified condition; however, the lower flowrate in upward flow improved the stratification. Higher HTF temperatures around the upper portion of the cylinders (i.e., T_{HTF3}) created by the stratified flow, offered stronger driving forces for charging PCMs relative to the mixed flow. Such factors for enhancing heat transfer rates were found relatively more apparent with lower flowrates, as the temperature difference between T_{HTF2} and T_{HTF3}, interpreted as the driving force for a stratified flow, diminished less rapidly with $\dot{V}_{HTF}$ of 0.5 m^3/h than 1.5 m^3/h (see Fig. 7).

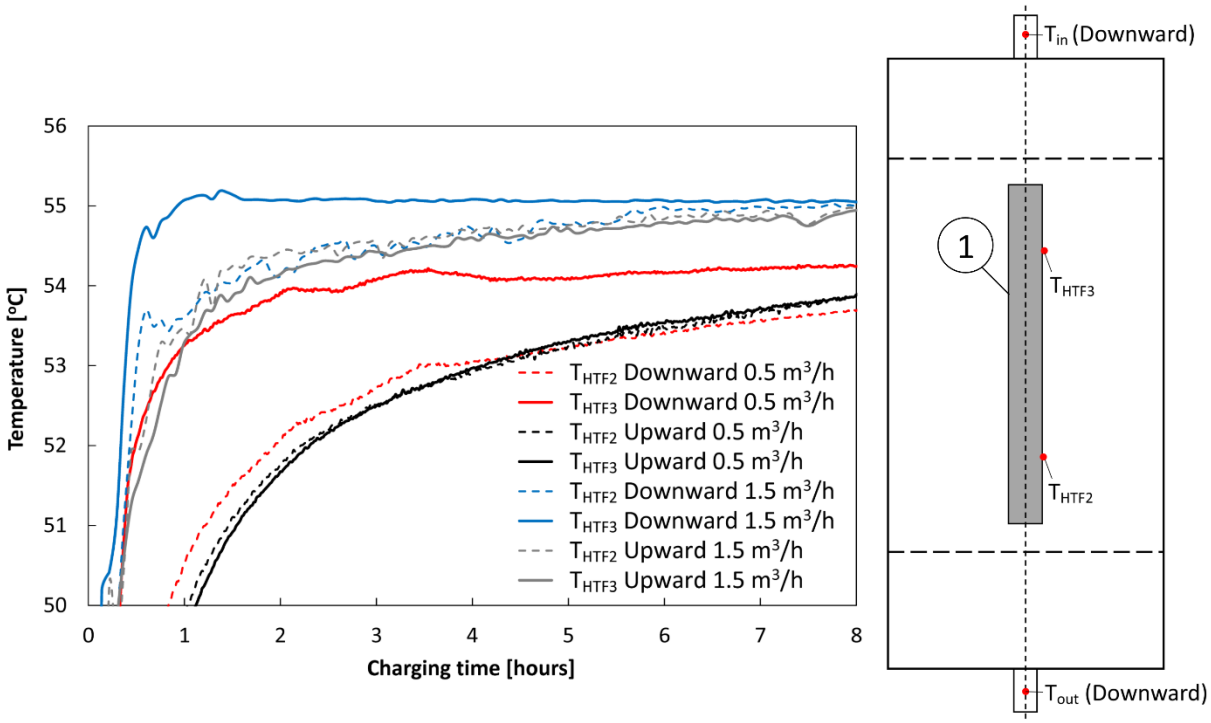

Fig. 7. Longitudinal HTF temperature distribution with upward and downward flow ($T_{HTF,spl}$ = 55 °C; $T_{TES,ini}$ = 35 °C) with vertical LHTES orientation.

Reflected in the charging time, stratification improved charging rates in PCMs, as presented in Table 5. Here, the time for Q_{PCM} to reach 75% and 90% of $Q_{PCM,theo}$, respectively, for two different flowrates and the two possible flow directions are presented. Relative to mixed flow (upward direction), the stratified flow (downward direction) with a lower flowrate ($\dot{V}_{HTF}$ = 0.5 m^3/h) produces a 52% decrease in charging time for a condition of 75% $Q_{PCM,theo}$. For the higher flow rate ($\dot{V}_{HTF}$ = 1.5 m^3/h), the same comparison indicates that time savings are reduced by only 21% on average. It is therefore vital to maintain a stratified tank by charging with downward HTF flow, especially for conditions with relatively low HTF flowrates.

Table 5 Charging time for PCM thermal capacity with two HTF flow directions and two flowrates ($T_{HTF,spl}$ = 55 °C; $T_{TES,ini}$ = 35 °C).

Parameters	**Test conditions**			
	$\dot{V}_{HTF}$ = 0.5 m^3/h		$\dot{V}_{HTF}$ of 1.5 m^3/h	
	Downward	Upward	Downward	Upward
$t\left(Q_{PCM,theo}^{75\%}\right)$ [hours]	4.4	9.2	2.8	3.5
$t\left(Q_{PCM,theo}^{90\%}\right)$ [hours]	9.1	18.9	5.2	6.7

4.2.Discharging mode

When discharging an LHTES unit for space heating, the HTF outlet temperature (T_{out}) should be sufficiently controlled to fulfill the supply-temperature requirement, which depends on the type of heating terminals and the outdoor temperatures. For the vertical LHTES orientation, maintaining a high T_{out} requires reducing $\dot{V}_{HTF}$, and thus a stratified flow regime (upward HTF flow for discharging) is necessary with $\dot{V}_{HTF}$ < 0.5 m^3/h. The evolution of T_{out} and of discharging rates (P_{TES}) is shown in Figs. 8(a) and (b), respectively, for six individual test conditions, with fixed $T_{HTF,spl}$ and $T_{TES,ini}$ (35 and 55 °C, respectively) and six values of $\dot{V}_{HTF}$ in range between 0.15 m^3/h to 4.0 m^3/h. In Fig. 8(a), the discharging time during which T_{out} was greater than 45 °C decreased significantly from 3.2 to 0.1 hours as $\dot{V}_{HTF}$ increased from 0.15 m^3/h to 4.0 m^3/h (*Re* increased from 22 to 575). The temperature threshold of 45 °C is chosen based on the standard rating condition for medium-temperature space heating applications [49].

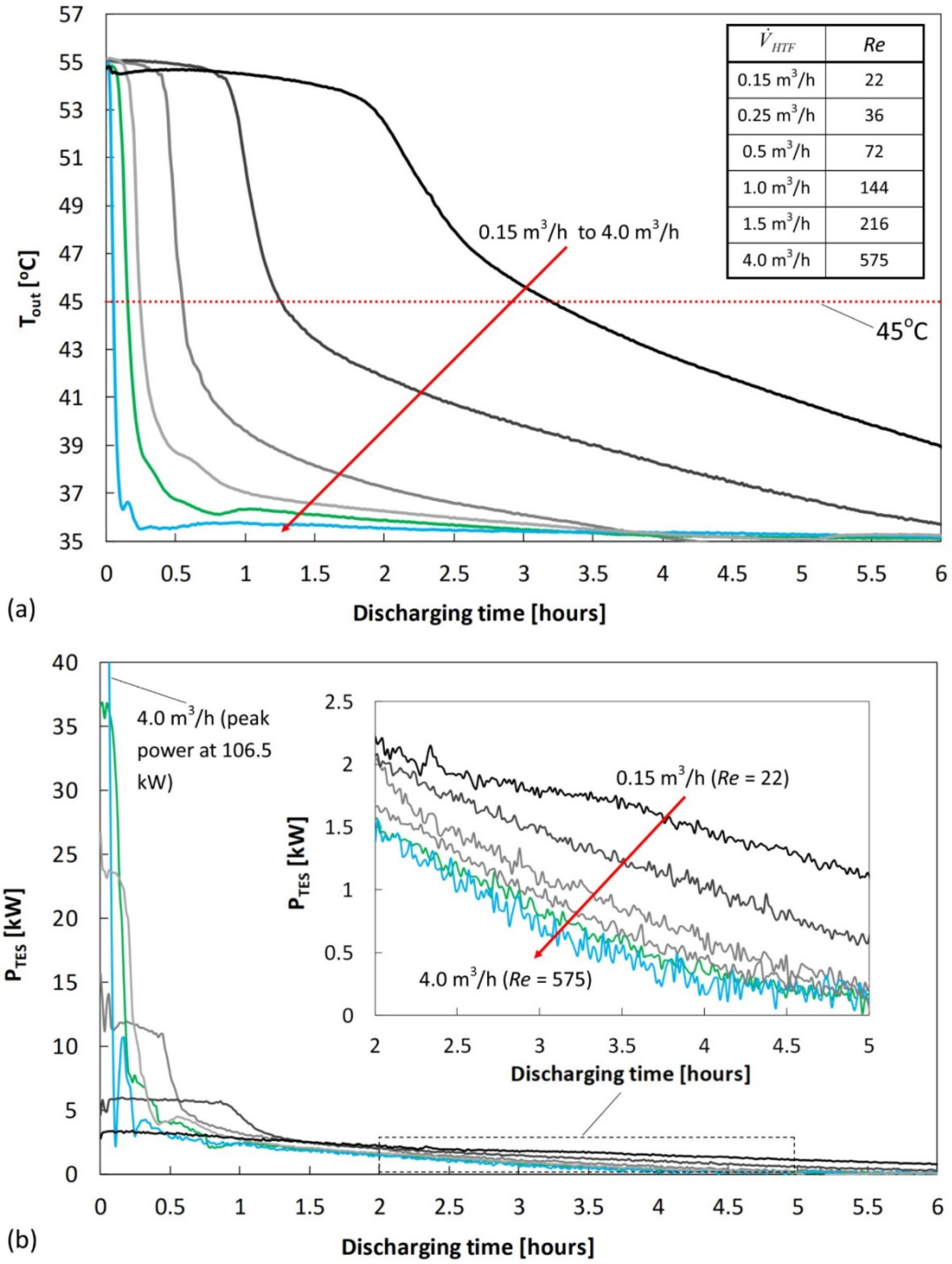

413

414 **Fig. 8.** Discharging outlet conditions with different HTF flowrates ($T_{HTF,spl}$ = 35 °C; $T_{TES,ini}$ = 55 °C) for the

415 vertical LHTES orientation: (a) HTF outlet temperature; (b) discharging rates.

416

Interestingly, high $\dot{V}_{HTF}$ does not necessarily lead to high P_{TES} throughout the entire discharging process. As shown in Fig. 8(b), P_{TES} for $\dot{V}_{HTF}$ = 0.15 m^3/h, the lowest tested flowrate, declined more slowly and at a higher level relative to the other conditions with higher flowrates after 2-hours of discharging. In contrast, with a high volumetric flowrate ($\dot{V}_{HTF}$ = 4.0 m^3/h, for instance), fresh HTF (water) rapidly flushed the previously stored water in the tank (within six minutes), creating peak P_{TES} in the initial discharging period. This initial condition was followed by slumps of T_{out} and P_{TES} because of the completion of water replacement. Subsequently, P_{TES} was the lowest for $\dot{V}_{HTF}$ = 4.0 m^3/h compared to that for lower flowrates. This finding can be ascribed to two aspects. First, as the flow remains in the laminar region, increasing HTF flowrates/Re brings no detectable improvement in convective heat transfer over the encapsulation surface. Second, the low thermal conductivity of the PCMs, together with the large diameter of the cylinder, impedes PCM solidification and, thus, heat removal. As a result, when compared to the reference discharging condition ($\dot{V}_{HTF}$ = 1.5 m^3/h), the test condition with $\dot{V}_{HTF}$ = 0.15 m^3/h results in 60% higher Q_{TES} based on the criteria of HTF temperature above 45 °C. That means low volumetric flowrates with stratification can provide a longer lasting high-temperature HTF output, together with a larger discharged thermal capacity with that high quality, when the LTHES unit releases heat continuously to heating terminals in a building.

4.3.Comparisons between vertical and horizontal orientation tests

With downward and upward HTF flow enabled by the vertical orientation of the LHTES unit, the thermal performance differed from that of the horizontal orientation. There are mainly two differences. First, the completely-charged/discharged Q_{PCM} is lower for the vertical orientation. As shown in Table 6, a comparison of key thermal-performance indicators reveals that under reference conditions with horizontal, downward, and upward HTF flow, Q_{PCM}

dropped by 5.9%/7.1% with downward/upward flow for charging and 8.2%/5.9% for discharging, respectively, compared to the horizontal. For both vertical directions, decreased Q_{PCM} led to consequent reductions in Q_{TES} and q_{TES} by at most 5.3%.

Table 6 Comparisons of thermal performance between vertical and horizontal orientation tests ($T_{HTF,spl}$ = 35 °C, $T_{TES,ini}$ = 55 °C, and $\dot{V}_{HTF}$ = 1.5 m^3/h).

Parameters	Charging			Discharging		
	Horizontal	Downward	Upward	Horizontal	Downward	Upward
$Q_{PCM,com}$ [kWh]	8.5	8.0	7.9	8.5	7.8	8.0
$\Delta Q_{PCM,com}$ [a] [%]	-	-5.9%	-7.1%	-	-8.2%	-5.9%
$Q_{TES,com}$ [kWh]	13.3	13.0	12.8	13.5	12.6	13.0
$\Delta Q_{TES,com}$ [b] [%]	-	-2.3%	-3.8%	-	-5.3%	-2.3%
$q_{TES,com}$ [kWh/m^3]	34.8	34.0	33.5	35.2	33.0	34.0
$t_{c,com}/t_{d,com}$ [hours]	8.2	6.6	7.5	8.3	6.7	6.2
$t(q_{TES}^{30\ kWh/m^3})$ [hours]	3.6	2.9	4.0	2.9	3.2	2.5

[a, b] Compared to the horizontal orientation.

On the other hand, the time for q_{TES} to reach 30.0 kWh/m^3 does not necessarily decrease in situations where $q_{TES,com}$ declined. For charging, the time was reduced from 3.6 to 2.9 hours, approximately 20%, for downward flow but was increased to 4.0 hours with the upward flow. This same time increased from 2.9 to 3.2 hours (+10%) when upward flow was supplied to the unit during discharging; however, it decreased to 2.5 hours (-14%) with the downward

flow. Such comparisons clearly show how a stratified flow regime with a vertical orientation is superior for producing shorter charging/discharging time, despite the reported loss in charged/discharged thermal capacity.

The second significance difference between the two orientations appeared in the PCM temperature distribution in the central PCM cylinder (i.e. PCM cylinder 1 in Fig. 1b). The evolution of PCM temperatures T_{PCM1} to T_{PCM4} with equivalent temperature and flowrate test conditions ($T_{HTF,spl}$ = 60 °C, $T_{TES,ini}$ = 35 °C, and $\dot{V}_{HTF}$ = 1.5 m^3/h), but with different HTF flow directions (horizontal and upward HTF flow respectively), are shown in Fig. 9. Here, T_{PCM1} and T_{PCM2} are nearly equivalent, whereas T_{PCM3} and T_{PCM4} differ significantly for the two different flow modes. When the cylinder was positioned vertically and supplied with upward flow during charging, the top end of the cylinder, where T_{PCM3} and T_{PCM4} were measured, experienced a more rapid temperature rise compared to the case in which the cylinder was oriented horizontally. Such behaviors have also been observed with other test conditions involving different values of $\dot{V}_{HTF}$ and $T_{HTF,spl}$.

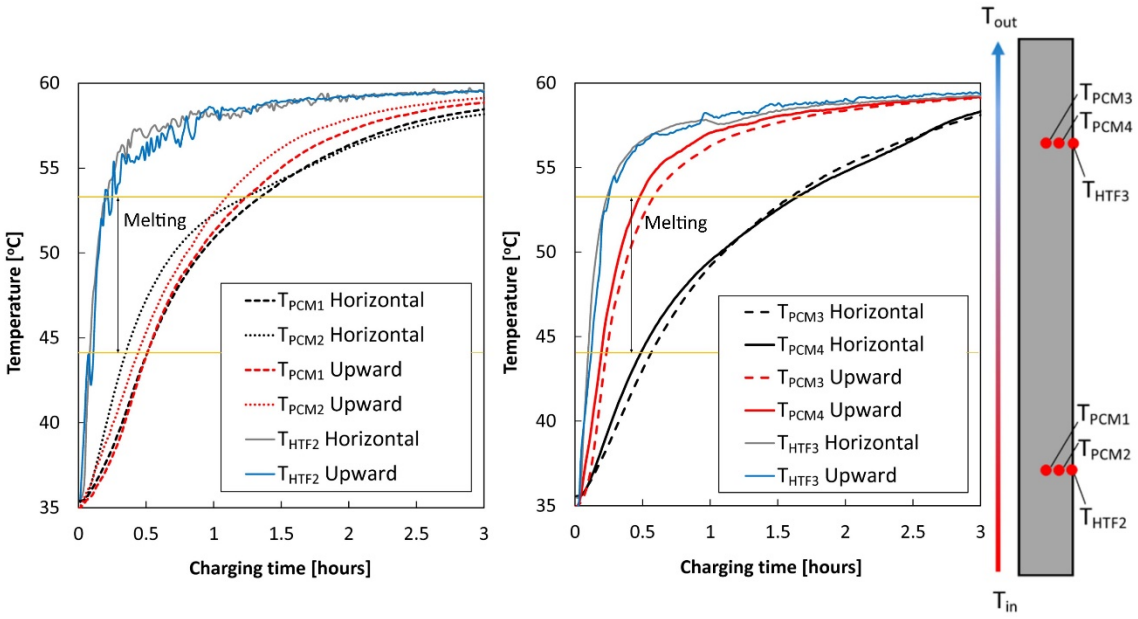

Fig. 9. PCM and HTF temperature evolution for PCM cylinder 1 with horizontal and upward flow during charging ($T_{HTF,spl}$ = 60 °C, $T_{TES,ini}$ = 35 °C, and $\dot{V}_{HTF}$ = 1.5 m^3/h).

The transient temperatures in Fig. 9 are suggestive of PCM behavior resulting from phase change. Under the condition that a cylinder in the test apparatus can be considered a long cylinder (L/D >10), axial conduction is negligible. Given that T_{HTF3}, which measured the HTF temperature at the same axial position as T_{PCM3} and T_{PCM4}, experienced minor temperature differences between horizontal and vertical orientation, ascending liquids in the cylinder were speculated to account for the rapid temperature rise of T_{PCM3} and T_{PCM4}. However, liquid PCM gel is supposed to exhibit high viscosity [50] and, thus, convective heat transfer has been shown to be negligible in several previous studies [47, 48]. Melted PCMs were hence unlikely to be transported to the upper regions of the cylinder by natural convection in a massive and rapid manner. However, Fig. 9(b) suggests that core PCM had completely melted by approximately 0.5 hour at the upper region but just started to melt at the bottom due to natural convection.

In light of two experimental observations: (1) free liquids were observed in encapsulated cylinders after the cylinders were installed vertically in the tank and tested; and (2) a loss in PCM thermal capacity of 5.9% – 8.2% was detected in the vertical orientation tests, it is inferred that the main cause of this seemingly natural-convection phenomenon is likely to be phase segregation. C48 is an incongruent melting PCM based on sodium acetate [51]. Though formulated with gelling agents, it may tend to separate after phase change, possibly in a relatively larger scale in this case due to a large vertical distance [52], i.e., the cylinder's length (750 mm) when it is vertically orientated. Assuming the gelling agent failed to hold the different phases of water and anhydrous salts originating from the incongruent melting, the separated water, when heated, could have ascended and produced the natural-convection-like behavior. In contrast, the horizontal cylinder is a more shallow container (69 mm diameter); in this arrangement the gelling agents are expected to restrain the bulk PCMs more effectively within such a small distance. The PCM's long-term stability may be at risk leading to continuous reduction in storage capacity [7], if phase segregation inevitably happened with vertical LHTES orientation.

5. Conclusions

The present study contributes to the development and the experimental investigation of a latent heat thermal energy storage (LHTES) unit containing a representative scale of cylindrically macro-encapsulated phase change materials (PCMs). The LHTES unit is expected to be integrated with space heating systems for heating load management. Findings from the present work can be summarized as follows:

(1) A parametric study on the supply temperature and the flowrate of heat transfer fluids (HTFs) is conducted for an LHTES in a horizontal orientation. Increasing the difference between HTF supply temperatures and phase-change temperatures accelerates the

506 charging/discharging process. The complete charging time and the time for the LHTES's
507 storage density to reach 30 kWh/m^3 is reduce by 14% and 61%, respectively, when the
508 HTF supply temperature is increased from 55 to 60 °C. During discharging, these same
509 times decrease by 42% and 52% when decreasing the HTF supply temperature from 35 to
510 30 °C, respectively.

511 Increasing the volumetric flowrate of the HTF also improves charging/discharging rates,
512 e.g., the complete charging/discharging time decreases by 14% and 13% when increasing
513 the HTF volumetric flowrate from 1.5 to 4.0 m^3/h, respectively.

514 (2) Charging/discharging rates in PCMs are summarized in performance maps covering all
515 completed test conditions in the horizontal orientation. The maps reveal a general non-
516 linearity of charging/discharging rates in PCMs after 75% of their theoretical thermal
517 capacity has been stored/released. The charging/discharging time can be reduced on
518 average by about 50%/30% if 75%/90% rather than 99% of the stored/released PCM
519 maximum thermal capacity is targeted, indicating that more than 50% of the
520 charging/discharging time can be saved if storing/recovering heat in PCMs with 75% of
521 its theoretical capacity instead of 99%.
522 (3) Placing the LHTES unit in a vertical orientation eliminates the flow distribution problem,
523 which is observed with an HTF volumetric flowrate of 0.5 m^3/h (Re = 72) in the
524 horizontal orientation tests. A stratified flow regime, formed by downward HTF flow,
525 improves charging rates in PCMs compared to the mixed flow regime; the charging time
526 for storing 90% of theoretical PCM capacity decreases by 21% with a flowrate of 1.5 m^3/h,
527 and more significantly, by 52% with a flowrate of 0.5 m^3/h due to better stratification.

528 When discharging the unit with stratified HTF flow at 35 °C, the lowest HTF flowrate
529 ($\dot{V}_{HTF}$ = 0.15 m^3/h, Re = 22) is favored for producing the longest discharging time (3.2

hours) during which the HTF outlet temperature is above 45 °C. These conditions also provide the highest discharging rate after two hours of discharging and the largest discharged thermal capacity with high HTF outlet temperature, compared to other higher flowrates up to 4.0 m^3/h (*Re* = 575). Delivering the released heat from the LHTES unit to heating terminals may require low HTF flowrates due to the requirement on the unit's outlet temperature.

(4) The vertical orientation of the LHTES unit exhibits advantages and disadvantages compared to the horizontal orientation. Although both the complete charging/discharging time and the time for the unit's energy density to reach 30 kWh/m^3 are reduced by around 20% with stratified flow, the charged/discharged PCM thermal capacity decreases by 8.2% at most when the unit is positioned vertically. The decrease in thermal capacity, together with the observed fluid motions in gelled PCMs, may indicate the occurrence of phase segregation with vertical LHTES orientation.

Suggested future work can include generalizing these experimental findings through a non-dimensional analysis and optimizing the PCM encapsulation geometries for improving heat transfer rates.

Acknowledgements

The test facility was financially supported by the Swedish Energy Agency. Tianhao Xu would like to thank the Chinese Scholarship Council (CSC) for his PhD stipend. Heartfelt gratitude is expressed to Prof. Viktoria Martin for her invaluable advice. The authors would like to sincerely express their gratitude to Prof. Tim Ameel for his great help in proofreading. Dr. Chen Xia is also thanked for his assistance in scientific writing. The authors would also like to thank Loris Tomasi, Dr. Muhammad Hamayun Maqbool, and Salvatore Piscopiello for their contributions to the experimental work.

Reference

[1] "Directive 2010/31/EU of the European parliament and of the council of 19 May 2010 on the energy performance of buildings."

[2] P. Bertoldi and B. Atanasiu, "Electricity consumption and efficiency trends in the enlarged European Union," *IES–JRC. European Union*, 2007.

[3] A. Arteconi, N. J. Hewitt, and F. Polonara, "State of the art of thermal storage for demand-side management," *Applied Energy*, vol. 93, pp. 371-389, 2012/05/01/ 2012.

[4] J. Heier, C. Bales, and V. Martin, "Combining thermal energy storage with buildings – a review," *Renewable and Sustainable Energy Reviews*, vol. 42, pp. 1305-1325, 2// 2015.

[5] J. P. E. K. C. Torvestad, "Nordic heating and cooling," Nordic Council of Ministers2017.

[6] A. Arteconi, N. J. Hewitt, and F. Polonara, "Domestic demand-side management (DSM): Role of heat pumps and thermal energy storage (TES) systems," *Applied Thermal Engineering*, vol. 51, pp. 155-165, 3// 2013.

[7] M. M. Farid, A. M. Khudhair, S. A. K. Razack, and S. Al-Hallaj, "A review on phase change energy storage: materials and applications," *Energy Conversion and Management*, vol. 45, pp. 1597-1615, 2004/06/01/ 2004.

[8] I. Dincer and M. Rosen, *Thermal energy storage: systems and applications*: John Wiley & Sons, 2002.

[9] P.-O. Johansson, *Buildings and district heating-contributions to development and assessments of efficient technology*, 2011.

[10] M. Jangsten, J. Kensby, J. O. Dalenbäck, and A. Trüschel, "Survey of radiator temperatures in buildings supplied by district heating," *Energy*, vol. 137, pp. 292-301, 2017/10/15/ 2017.

[11] S. Frederiksen and S. Werner, *District heating and cooling*: Studentlitteratur, 2013.

[12] F. Karlsson, *Capacity control of residential heat pump heating systems*, 2007.

[13] L. F. Cabeza, A. Castell, C. Barreneche, A. de Gracia, and A. I. Fernández, "Materials used as PCM in thermal energy storage in buildings: A review," *Renewable and Sustainable Energy Reviews*, vol. 15, pp. 1675-1695, 4// 2011.

[14] J. N. Chiu, V. Martin, and F. Setterwall, "A review of thermal energy storage systems with salt hydrate phase change materials for comfort cooling," in *EFFSTOCK 2009*, 2009.

[15] L. F. Cabeza, G. Svensson, S. Hiebler, and H. Mehling, "Thermal performance of sodium acetate trihydrate thickened with different materials as phase change energy storage material," *Applied Thermal Engineering*, vol. 23, pp. 1697-1704, 9// 2003.

[16] M. K. A. Sharif, A. A. Al-Abidi, S. Mat, K. Sopian, M. H. Ruslan, M. Y. Sulaiman, *et al.*, "Review of the application of phase change material for heating and domestic hot water systems," *Renewable and Sustainable Energy Reviews*, vol. 42, pp. 557-568, 2// 2015.

[17] Z. N. Meng and P. Zhang, "Experimental and numerical investigation of a tube-in-tank latent thermal energy storage unit using composite PCM," *Applied Energy*, vol. 190, pp. 524-539, 2017/03/15/ 2017.

[18] M. Dannemand, J. B. Johansen, W. Kong, and S. Furbo, "Experimental investigations on cylindrical latent heat storage units with sodium acetate trihydrate composites utilizing supercooling," *Applied Energy*, vol. 177, pp. 591-601, 2016/09/01/ 2016.

[19] P. B. Salunkhe and P. S. Shembekar, "A review on effect of phase change material encapsulation on the thermal performance of a system," *Renewable and Sustainable Energy Reviews*, vol. 16, pp. 5603-5616, 2012/10/01/ 2012.

[20] F. Agyenim and N. Hewitt, "The development of a finned phase change material (PCM) storage system to take advantage of off-peak electricity tariff for improvement in cost of heat pump operation," *Energy and Buildings,* vol. 42, pp. 1552-1560, 9// 2010.

[21] V. Martin and F. Setterwall, "Compact Heat Storage for Solar Heating Systems," *Journal of Solar Energy Engineering,* vol. 131, pp. 041011-041011-6, 2009.

[22] M. J. Hosseini, A. A. Ranjbar, M. Rahimi, and R. Bahrampoury, "Experimental and numerical evaluation of longitudinally finned latent heat thermal storage systems," *Energy and Buildings,* vol. 99, pp. 263-272, 2015/07/15/ 2015.

[23] M. K. Rathod and J. Banerjee, "Thermal performance enhancement of shell and tube Latent Heat Storage Unit using longitudinal fins," *Applied Thermal Engineering,* vol. 75, pp. 1084-1092, 1/22/ 2015.

[24] M. Avci and M. Y. Yazici, "Experimental study of thermal energy storage characteristics of a paraffin in a horizontal tube-in-shell storage unit," *Energy Conversion and Management,* vol. 73, pp. 271-277, 9// 2013.

[25] J. P. da Cunha and P. Eames, "Compact latent heat storage decarbonisation potential for domestic hot water and space heating applications in the UK," *Applied Thermal Engineering,* vol. 134, pp. 396-406, 2018/04/01/ 2018.

[26] R. Waser, F. Ghani, S. Maranda, T. S. O'Donovan, P. Schuetz, M. Zaglio, *et al.*, "Fast and experimentally validated model of a latent thermal energy storage device for system level simulations," *Applied Energy,* vol. 231, pp. 116-126, 2018/12/01/ 2018.

[27] M. J. Hosseini, M. Rahimi, and R. Bahrampoury, "Experimental and computational evolution of a shell and tube heat exchanger as a PCM thermal storage system," *International Communications in Heat and Mass Transfer,* vol. 50, pp. 128-136, 2014/01/01/ 2014.

628 [28] X. Xiao and P. Zhang, "Numerical and experimental study of heat transfer
629 characteristics of a shell-tube latent heat storage system: Part I – Charging process,"
630 *Energy,* vol. 79, pp. 337-350, 1/1/ 2015.
631 [29] X. Xiao and P. Zhang, "Numerical and experimental study of heat transfer
632 characteristics of a shell-tube latent heat storage system: Part II – Discharging
633 process," *Energy*, vol. 80, pp. 177-189, 2/1/ 2015.
634 [30] P. Zhang, F. Ma, and X. Xiao, "Thermal energy storage and retrieval characteristics of
635 a molten-salt latent heat thermal energy storage system," *Applied Energy,* vol. 173, pp.
636 255-271, 7/1/ 2016.
637 [31] T. Nuytten, P. Moreno, D. Vanhoudt, L. Jespers, A. Solé, and L. Cabeza,
638 "Comparative analysis of latent thermal energy storage tanks for micro-CHP systems,"
639 *Applied Thermal Engineering,* vol. 59, pp. 542-549, 2013.
640 [32] J. P. Bédécarrats, J. Castaing-Lasvignottes, F. Strub, and J. P. Dumas, "Study of a
641 phase change energy storage using spherical capsules. Part I: Experimental results,"
642 *Energy Conversion and Management,* vol. 50, pp. 2527-2536, 10// 2009.
643 [33] M.-J. Li, B. Jin, Z. Ma, and F. Yuan, "Experimental and numerical study on the
644 performance of a new high-temperature packed-bed thermal energy storage system
645 with macroencapsulation of molten salt phase change material," *Applied Energy*, vol.
646 221, pp. 1-15, 2018/07/01/ 2018.
647 [34] N. Nallusamy, S. Sampath, and R. Velraj, "Experimental investigation on a combined
648 sensible and latent heat storage system integrated with constant/varying (solar) heat
649 sources," *Renewable Energy,* vol. 32, pp. 1206-1227, 6// 2007.
650 [35] S. Bellan, T. E. Alam, J. González-Aguilar, M. Romero, M. M. Rahman, D. Y.
651 Goswami, *et al.*, "Numerical and experimental studies on heat transfer characteristics

of thermal energy storage system packed with molten salt PCM capsules," *Applied Thermal Engineering*, vol. 90, pp. 970-979, 11/5/ 2015.

[36] X. Cheng and X. Zhai, "Thermal performance analysis and optimization of a cascaded packed bed cool thermal energy storage unit using multiple phase change materials," *Applied Energy*, vol. 215, pp. 566-576, 2018/04/01/ 2018.

[37] C. Arkar and S. Medved, "Influence of accuracy of thermal property data of a phase change material on the result of a numerical model of a packed bed latent heat storage with spheres," *Thermochimica Acta*, vol. 438, pp. 192-201, 2005/11/01/ 2005.

[38] N. Nallusamy and R. Velraj, "Numerical and Experimental Investigation on a Combined Sensible and Latent Heat Storage Unit Integrated With Solar Water Heating System," *Journal of Solar Energy Engineering*, vol. 131, pp. 041002-041002-8, 2009.

[39] P. Moreno, A. Castell, C. Solé, G. Zsembinszki, and L. F. Cabeza, "PCM thermal energy storage tanks in heat pump system for space cooling," *Energy and Buildings*, vol. 82, pp. 399-405, 10// 2014.

[40] J. Wei, Y. Kawaguchi, S. Hirano, and H. Takeuchi, "Study on a PCM heat storage system for rapid heat supply," *Applied Thermal Engineering*, vol. 25, pp. 2903-2920, 2005/12/01/ 2005.

[41] Climator. (2018, 2018-12-02). *C48 Datasheet*. Available: https://www.climator.com/images/pdf/prodblad_climsel_c48_4.1.pdf

[42] YOKOGAWA. (2018-10-21). *RXF Magnetic Flowmeter User's Manual*. Available: https://www.yokogawa.com/pl/product/rxf/RXF_IM_01R21D01_01E_E_01.pdf

[43] YOKOGAWA. (2018-10-21). *Model EJA110A, EJA120A and EJA130A, Differential Pressure Transmitters, User's Manual*. Available: https://web-material3.yokogawa.com/IM01C21B01-01EN_011_1.pdf

[44] B. N. Taylor and C. E. Kuyatt, "Guidelines for evaluating and expressing the uncertainty of NIST measurement results," 1994.

[45] C. E. Systems. Available: http://www.cristopia.com/EN/Public/fr-FR/catalogue.pdf

[46] P. P. Ltd. Available: http://www.pcmproducts.net/Building_Temperature_Control.htm

[47] J. N. W. Chiu and V. Martin, "Submerged finned heat exchanger latent heat storage design and its experimental verification," *Applied Energy*, vol. 93, pp. 507-516, 2012/05/01/ 2012.

[48] A. Saito, S. Okawa, T. Shintani, and R. Iwamoto, "On the heat removal characteristics and the analytical model of a thermal energy storage capsule using gelled Glauber's salt as the PCM," *International Journal of Heat and Mass Transfer*, vol. 44, pp. 4693-4701, 2001/12/01/ 2001.

[49] *Air conditioners, liquid chilling packages and heat pumps with electrically driven compressors for space heating and cooling - Part 2: Test conditions*, S. S. Institute, 2013.

[50] G. Lane, "Solar heat storage: Latent heat materials. Volume II. Technology," Dow Chemical Co., Midland, MI1986.

[51] S. N. Gunasekara, V. Martin, and J. N. Chiu, "Phase equilibrium in the design of phase change materials for thermal energy storage: State-of-the-art," *Renewable and Sustainable Energy Reviews*, vol. 73, pp. 558-581, 6// 2017.

[52] H. Mehling and L. F. Cabeza, *Heat and cold storage with PCM* vol. 308: Springer.

Figure Captions

Fig. 1. Illustration of LHTES unit and encapsulated PCM cylinders.

Fig. 2. Schematic diagram of the test facility.

Fig. 3. PCM temperature measurement positions in metallic PCM cylinders.

Fig. 4. The evolution of PCM temperature and charged thermal capacity with different HTF supply conditions for charging: (a) $T_{HTF,spl}$ of 55, 58 and, 60 °C at 1.5 m^3/h ($T_{TES,ini}$ at 35 °C); (b) $\dot{V}_{HTF}$ of 0.5, 1.5 and, 4.0 m^3/h with $T_{HTF,spl}$ of 55 °C ($T_{TES,ini}$ at 35 °C).

Fig. 5. The evolution of PCM temperature and discharged thermal capacity with different HTF supply conditions for discharging: (a) $T_{HTF,spl}$ of 30, 35, and 40 °C at 1.5 m^3/h ($T_{TES,ini}$ at 55 °C); (b) $\dot{V}_{HTF}$ of 0.5, 1.5, and 4.0 m^3/h with $T_{HTF,spl}$ of 35 °C ($T_{TES,ini}$ at 55 °C).

Fig. 6. Generalized performance map of charging/discharging rates in PCMs with horizontal LHTES orientation: (a) charging; (b) discharging.

Fig. 7. Longitudinal HTF temperature distribution with upward and downward flow ($T_{HTF,spl}$ = 55 °C; $T_{TES,ini}$ = 35 °C) with vertical LHTES orientation.

Fig. 8. Discharging outlet conditions with different HTF flowrates ($T_{HTF,spl}$ = 35 °C; $T_{TES,ini}$ = 55 °C) for the vertical LHTES orientation: (a) HTF outlet temperature; (b) discharging rates.

Fig. 9. PCM and HTF temperature evolution for PCM cylinder 1 with horizontal and upward flow during charging ($T_{HTF,spl}$ = 60 °C, $T_{TES,ini}$ = 35 °C, and $\dot{V}_{HTF}$ = 1.5 m^3/h).

Table Captions

Table 1 Thermo-physical properties of Climsel C48 [55].

Table 2 Uncertainty analysis for charging/discharging rates and thermal capacity.

Table 3 Charging thermal performance with different test conditions for the horizontal LHTES orientation.

Table 4 Discharging thermal performance with different test conditions for the horizontal LHTES orientation.

Table 5 Charging time for PCM thermal capacity with two HTF flow directions and two flowrates ($T_{HTF,spl}$ = 55 °C; $T_{TES,ini}$ = 35 °C).

Table 6 Comparisons of thermal performance between vertical and horizontal orientation tests ($T_{HTF,spl}$ = 35 °C, $T_{TES,ini}$ = 55 °C, and $\dot{V}_{HTF}$ = 1.5 m^3/h).